Resonance Raman Studies of the Iron(II)−α-Keto Acid Chromophore in Model and Enzyme Complexes

ARTICLE *in* JOURNAL OF THE AMERICAN CHEMICAL SOCIETY · JUNE 2001

Impact Factor: 12.11 · DOI: 10.1021/ja0041775 · Source: PubMed

Resonance Raman Studies of the Iron(II)−α-Keto Acid Chromophore in Model and Enzyme Complexes

Raymond Y. N. Ho,[†] Mark P. Mehn,[†] Eric L. Hegg,[†,⊥] Aimin Liu,[†] Matthew J. Ryle,[‡] Robert P. Hausinger,[‡] and Lawrence Que, Jr.*,[†]

Contribution from the Department of Chemistry and Center for Metals in Biocatalysis, 207 Pleasant Street SE, University of Minnesota, Minneapolis, Minnesota 55455, and Departments of Microbiology & Molecular Genetics and Biochemistry & Molecular Biology, Michigan State University, East Lansing, Michigan 48824

Received December 5, 2000

Abstract: The bidentate coordination of an α-keto acid to an iron(II) center via the keto group and the carboxylate gives rise to metal-to-ligand charge-transfer transitions between 400 and 600 nm in model complexes and in α-ketoglutarate-dependent dioxygenases. Excitation into these absorption bands of the Fe(II)TauD(α-KG) complex (TauD = taurine/α-ketoglutarate dioxygenase, α-KG = α-ketoglutarate) elicits two resonance Raman features at 460 and 1686 cm^{-1}, both of which are sensitive to ^{18}O labeling. Corresponding studies of model complexes, the six-coordinate [Fe(II)(6-Me_3-TPA)(α-keto acid)]$^+$ and the five-coordinate [Fe(II)(Tp^{Ph2})(α-keto acid)] (6-Me_3-TPA = tris[(6-methyl-2-pyridyl)methyl]amine, Tp^{Ph2} = hydrotris(3,5-diphenylpyrazol-1-yl)borate), lead to the assignment of these two features to the Fe(II)(α-keto acid) chelate mode and the ν(C═O) of the keto carbonyl group, respectively. Furthermore, the chelate mode is sensitive to the coordination number of the metal center; binding of a sixth ligand to the five-coordinate [Fe(II)(Tp^{Ph2})(benzoylformate)] elicits a 9−20 cm^{-1} downshift. Thus, the 10 cm^{-1} upshift of the chelate mode observed for Fe(II)TauD(α-KG) upon the addition of the substrate, taurine, is associated with the conversion of the six-coordinate metal center to a five-coordinate center, as observed for the iron center of clavaminate synthase from X-ray crystallography (Zhang, Z.; et al. *Nat. Struct. Biol.* **2000**, *7*, 127−133) and MCD studies (Zhou, J.; et al. *J. Am. Chem. Soc.* **1998**, *120*, 13539−13540). These studies provide useful insights into the initial steps of the oxygen activation mechanism of α-ketoglutarate-dependent dioxygenases.

α-Ketoglutarate (α-KG)[1]-dependent dioxygenases constitute a large class of non-heme iron-containing enzymes that are essential for the biosynthesis of a diverse array of biological compounds and for the biodegradation of selected biomolecules.[2−5] Examples of these enzymes include prolyl hydroxylase, an enzyme that is important in collagen biosynthesis;[6] deacetoxycephalosporin C synthase (DAOCS), an enzyme that converts penicillins to cephalosporins;[7,8] clavaminate synthase 2 (CAS), an enzyme that is needed to synthesize the β-lactamase inhibitor clavulanic acid;[9] 2,4-dichlorophenoxyacetic acid (2,4-D)/α-KG dioxygenase (TfdA), an enzyme that degrades the herbicide 2,4-D;[10,11] and taurine/α-KG dioxygenase (TauD), an enzyme that allows *Escherichia coli* to utilize taurine as a sulfur source.[12,13] Despite the diversity of chemical transformations catalyzed, it is likely that there is a common iron active site with a 2-His-1-carboxylate facial triad,[14−17] and a common oxygen activation mechanism for α-keto acid-dependent enzymes has been proposed.[4,18,19] The first step of the proposed mechanism (Scheme 1) involves the binding of the α-KG cosubstrate to the iron(II) center, followed by substrate binding near the active site. O_2 binds to the iron center to afford an

* To whom correspondence should be addressed. E-mail: que@chem.umn.edu.

† University of Minnesota.

‡ Michigan State University.

⊥ Current address: Department of Chemistry, University of Utah, Salt Lake City, UT 84112.

(1) Abbreviations used: α-KG, α-ketoglutarate; CAS, clavaminate synthase 2; DAOCS, deacetoxycephalosporin C synthase; 2,4-D, 2,4-dichlorophenoxyacetic acid; TfdA, (2,4-D)/α-KG dioxygenase; TauD, taurine/α-KG dioxygenase; 6-Me_3-TPA, tris(6-methyl-2-pyridylmethyl)-amine; Tp^{Ph2}, hydrotris(3,5-diphenylpyrazol-1-yl)borate; BF, benzoylformate; PRV, pyruvate.

(2) De Carolis, E.; De Luca, V. *Phytochemistry* **1994**, *36*, 1093−1107.

(3) Prescott, A. G.; John, P. *Annu. Rev. Plant Physiol. Plant Mol. Biol.* **1996**, *47*, 245−271.

(4) Schofield, C. J.; Zhang, Z. *Curr. Opin. Struct. Biol.* **1999**, *9*, 722−731.

(5) Solomon, E. I.; Brunold, T. C.; Davis, M. I.; Kemsley, J. N.; Lee, S.-K.; Lehnert, N.; Neese, F.; Skulan, A. J.; Yang, Y.-S.; Zhou, J. *Chem. Rev.* **2000**, *100*, 235−349.

(6) Kivirikko, K. I.; Myllylä, R.; Pihlajaniemi, T. *FASEB J.* **1989**, *3*, 1609−1617.

(7) Baldwin, J. E.; Abraham, E. *Nat. Prod. Rep.* **1988**, *5*, 129−145.

(8) Baldwin, J. E.; Adlington, R. M.; Crouch, N. P.; Schofield, C. J.; Turner, N. J.; Aplin, R. T. *Tetrahedron* **1991**, *47*, 9881−9900.

(9) Salowe, S. P.; Marsh, E. N.; Townsend, C. A. *Biochemistry* **1990**, *29*, 6499−6508.

(10) Hogan, D. A.; Smith, S. R.; Saari, E. A.; McCracken, J.; Hausinger, R. P. *J. Biol. Chem.* **2000**, *275*, 12400−12409.

(11) Fukumori, F.; Hausinger, R. P. *J. Biol. Chem.* **1993**, *268*, 24311−24317.

(12) van der Ploeg, J. R.; Weiss, M. A.; Saller, E.; Nashimoto, H.; Saito, N.; Kertesz, M. A.; Leisinger, T. *J. Bacteriol.* **1996**, *178*, 5438−5446.

(13) Eichhorn, E.; van der Ploeg, J. R.; Kertesz, M. A.; Leisinger, T. *J. Biol. Chem.* **1997**, *272*, 23031−23036.

(14) Vålegard, K.; van Scheltinga, A. C. T.; Lloyd, M. D.; Hara, T.; Ramaswamy, S.; Perrakis, A.; Thompson, A.; Lee, H.-J.; Baldwin, J. E.; Schofield, C. J.; Hajdu, J.; Andersson, I. *Nature* **1998**, *394*, 805−809.

(15) Serre, L.; Sailland, A.; Sy, D.; Boudec, P.; Rolland, A.; Pebay-Peyroula, E.; Cohen-Addad, C. *Structure* **1999**, *7*, 977−988.

(16) Zhang, Z.; Ren, J.; Stammers, D. K.; Baldwin, J. E.; Harlos, K.; Schofield, C. J. *Nat. Struct. Biol.* **2000**, *7*, 127−133.

(17) Hegg, E. L.; Que, L., Jr. *Eur. J. Biochem.* **1997**, *250*, 625−629.

(18) Hanauske-Abel, H. M.; Günzler, V. *J. Theor. Biol.* **1982**, *94*, 421−455.

(19) Que, L., Jr.; Ho, R. Y. N. *Chem. Rev.* **1996**, *96*, 2607−2624.

10.1021/ja0041775 CCC: $20.00
Published on Web 05/04/2001

Scheme 1. Proposed Mechanism for α-KG-Dependent Non-Heme Iron Enzymes

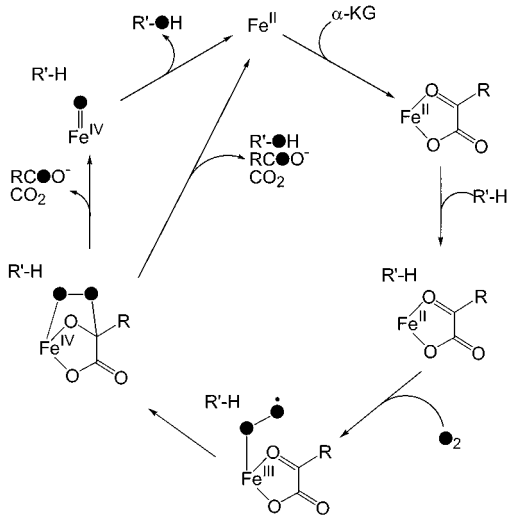

Fe(III) superoxide species. The superoxide then attacks the α-carbon of the bound α-keto acid to initiate oxidative decarboxylation of the α-KG and generates a species (either a peroxo or a high-valent iron−oxo moiety) which oxidizes the substrate.

The recently reported crystal structures of α-KG complexes of Fe(II)DAOCS[14] and Fe(II)CAS[16] show that α-KG binds to the iron center in a bidentate mode via the C-1 carboxylate oxygen and the α-keto carbonyl oxygen. This binding mode was anticipated by the observation of charge-transfer transitions around 500−600 nm upon addition of α-KG and Fe(II) to CAS,[20] TfdA,[21] and TauD.[22] On the basis of earlier model studies of Fe(II)−α-keto acid complexes, these metal-to-ligand charge-transfer transitions arise only when the α-keto acid binds to the iron in such a bidentate mode.[23] Resonance Raman spectroscopy has been shown to be a good probe of charge-transfer transitions[24] and can provide more detailed insight into the nature of the chromophore. We present here the first resonance Raman studies of the iron(II)−α-keto acid chromophore in model complexes and use these observations to interpret the Raman data for the α-KG-dependent enzyme, TauD. These results support the initial steps in the proposed oxygen activation mechanism of α-KG-dependent enzymes.

Experimental Section

General Materials and Procedures. All reagents and solvents were purchased from commercial sources and were used without further purification unless otherwise noted. Methanol was distilled from Mg(OMe)$_2$ before use. Labeled water (either 95% ^{18}O or 85% ^{18}O containing 33% ^{2}H) was obtained from ICON, Inc. 6-Me$_3$-TPA and KTp^{Ph2} were synthesized according to published procedures.[25,26] Preparation and handling of air-sensitive materials were carried out under an inert atmosphere using standard Schlenk techniques or a glovebox. ***Caution!*** *Perchlorate salts are potentially explosive and should be handled with care.*

Preparation of TauD Samples. TauD was purified from *Escherichia coli* BL21 (DE3) [pME4141] according to the procedure of Ryle et al.[22] The Raman samples were prepared under argon from lyophilized apo-enzyme that was dissolved in pH 8 Tris buffer (25 mM) to give a final concentration of 2.6−3.2 mM. Fe(II)TauD was prepared by reconstitution of apo-enzyme with 1 equiv (relative to TauD subunit) of Fe(II)(NH$_4$)$_2$(SO$_4$)$_2$ in H$_2$O, resulting in a sample with no visible chromophore. The binary Fe(II)TauD(α-KG) complex was prepared by adding 2 equiv (relative to TauD subunit) of the monosodium salt of α-ketoglutaric acid dissolved in pH 8 Tris buffer to a solution of Fe(II)TauD. The resulting purple solution was transferred anaerobically to a spinning cell filled with Ar. Samples of the ternary Fe(II)TauD-(α-KG)(taurine) complex were generated by adding 2 equiv (relative to TauD subunit) of taurine to the binary complex before transferring the solution to the spinning cell. The H$_2$^{18}O samples were prepared by using a similar procedure, except that the pH 8 buffer and Fe(II)(NH$_4$)$_2$-(SO$_4$)$_2$ were dissolved in H$_2$^{18}O (95% ^{18}O). The α-ketoglutaric acid was also dissolved in H$_2$^{18}O (95% ^{18}O) and allowed to equilibrate for 10 min prior to addition to the Fe(II)TauD solution. No decay of the purple color characteristic of the α-KG complex was observed during Raman acquisition. Upon acquisition of its Raman spectrum, each TauD sample was exposed to air for 30 min, during which time the purple chromophore decayed. The Raman spectra of these air-oxidized samples were then acquired for subtraction of the fluorescence background and the nonenhanced protein vibrations. In general, the percent subtraction was based on removing the protein deformation mode around 1450 cm^{-1}.

6-Me$_3$-TPA Complexes. [Fe(II)(6-Me$_3$-TPA)(BF)](ClO$_4$) was prepared according to the published procedure.[23] The UV/vis and ^{1}H NMR spectra were consistent with the published values.[23] [Fe(II)(6-Me$_3$-TPA)-(PRV)](ClO$_4$) was prepared in the following manner. To a methanolic solution of Fe(ClO$_4$)$_2$·8H$_2$O (0.25 mmol) and 6-Me$_3$-TPA (0.25 mmol) was added sodium pyruvate (0.25 mmol) under Ar. The resulting red-orange solution was stirred for 30 min, concentrated, and filtered. After solvent removal under vacuum, the solid red-orange [Fe(II)(6-Me$_3$-TPA)(PRV)](ClO$_4$) complex was obtained. Metathesis with NaBPh$_4$ in methanol afforded a solid (48% yield). ^{1}H NMR (CD$_3$CN) δ: 50.1 (4H), 46.7 (2H), 17.5 (3H), 15.9 (3H), 7.2 (20H), 1.94 (solv), −36.8 (9H). Anal. Calcd for C$_{48}$H$_{47}$BFeN$_4$O$_3$: C, 72.55; H, 5.97; N, 7.05. Found: C, 72.34; H, 6.04; N, 6.90.

Tp^{Ph2} Complexes. [Fe(II)(Tp^{Ph2})(BF)] was prepared through a modification of the reported procedure.[27] To a dry methanolic solution (15 mL) containing equimolar amounts of Fe(ClO$_4$)$_2$·8H$_2$O (1.0 mmol) and KTp^{Ph2} (1.0 mmol) was added 1 equiv of sodium benzoylformate (1.0 mmol). Upon addition of the α-keto acid, a purple solid precipitated. Filtration and washing of this solid with methanol gave a purple solid, the NMR and UV/vis spectra of which matched those previously reported.[27] [Fe(II)(Tp^{Ph2})(PRV)] was prepared in a manner analogous to that used for [Fe(II)(Tp^{Ph2})(BF)], except sodium pyruvate was used in place of sodium benzoylformate.

Labeled Compounds. Pyruvic-*1-^{13}C* acid and pyruvic-*2-^{13}C* acid were purchased as their sodium salts from Cambridge Isotope Laboratories, Inc., and used without further purification. Pyruvic acid was purified by vacuum distillation prior to use and stored at −20 °C in the dark to prevent decomposition or oligomerization.[28] ^{18}O-labeled pyruvate samples were prepared by acid-catalyzed exchange with "unnormalized" H$_2$^{18}O (85% ^{18}O containing 33% ^{2}H) according to the literature precedent.[29,30] This exchange was followed by ^{13}C NMR spectroscopy, since the ^{13}C shift is known to be sensitive to ^{16}O/^{18}O substitution.[31] A Shigemi tube with the susceptibility matched to that

(20) Pavel, E. G.; Zhou, J.; Busby, R. W.; Gunsior, M.; Townsend, C. A.; Solomon, E. I. *J. Am. Chem. Soc.* **1998**, *120*, 743−753.
(21) Hegg, E. L.; Whiting, A. K.; Saari, R. E.; McCracken, J.; Hausinger, R. P.; Que, L., Jr. *Biochemistry* **1999**, *38*, 16714−16726.
(22) Ryle, M. J.; Padmakumar, R.; Hausinger, R. P. *Biochemistry* **1999**, *38*, 15278−15286.
(23) Chiou, Y.-M.; Que, L., Jr. *J. Am. Chem. Soc.* **1995**, *117*, 3999−4013.
(24) Spiro, T. G.; Czernuszewicz, R. S. In *Physical Methods in Bioinorganic Chemistry. Spectroscopy and Magnetism*; Que, L., Jr., Ed.; University Science Books: Sausalito, CA, 2000; pp 59−120.
(25) DaMota, M. M.; Rodgers, J.; Nelson, S. M. *J. Chem. Soc. A* **1969**, 2036−2044.
(26) Kitajima, N.; Fujisawa, K.; Fujimoto, C.; Moro-oka, Y.; Hashimoto, S.; Kitagawa, T.; Toriumi, K.; Tatsumi, K.; Nakamura, A. *J. Am. Chem. Soc.* **1992**, *114*, 1277−1291.
(27) Hegg, E. L.; Ho, R. Y. N.; Que, L., Jr. *J. Am. Chem. Soc.* **1999**, *121*, 1972−1973.
(28) Margolis, S. A.; Coxon, B. *Anal. Chem.* **1986**, *58*, 2504−2510.
(29) Dyllick-Brenzinger, C. E.; Bauder, A.; Günthard, H. H. *Chem. Phys.* **1977**, *23*, 195−206.
(30) Hollenstein, H.; Akermann, F.; Günthard, H. H. *Spectrochim. Acta* **1978**, *34A*, 1041−1063.
(31) Jameson, C. J. *J. Chem. Phys.* **1977**, *66*, 4983−4988.

of D_2O was used to minimize the sample volume, and ^1H and ^{13}C NMR spectra were collected on a Varian VI-500 spectrometer at room temperature. The ^{13}C NMR spectra of the approximately 1.5 M pyruvic acid solutions that were allowed to equilibrate for 24 h reveal that ^{18}O substitution occurred at both the α-keto and carboxylate carbons. Attempts to label solely at the keto position using shorter time frames were unsuccessful. Therefore, long exchange times (1 week) were used to obtain "fully" ^{18}O-labeled pyruvic acid, which was shown by the ^{13}C NMR spectra to be mostly ^{18}O-labeled at both the α-keto carbonyl and carboxylate groups (Figures S1 and S2, Supporting Information). Benzoylformic acid was labeled in a similar manner. Due to its lower solubility in water, lower concentrations (~0.75 M) of benzoylformic acid were used, and longer times (2 weeks) were required for substantial ^{18}O incorporation (Figures S3 and S4, Supporting Information). No exchange with $H_2{}^{18}O$ was observed with the sodium salts of the α-keto acids. The ^{18}O-labeled complexes were prepared by neutralizing the α-keto acid with NaOH immediately prior to synthesis of the complexes described above.

$[Fe(II)(6\text{-}Me_3\text{-}TPA)(BF)]^+$ ^{18}O-labeled only at the α-keto carbonyl group was obtained by adding 100 equiv (based on iron complex) of $H_2{}^{18}O$ (95−97% ^{18}O) to a CH_3CN solution of $Fe(II)(6\text{-}Me_3\text{-}TPA)(BF)]^+$ (5−10 mM). This solution was allowed to equilibrate at room temperature for 30 min before a sample was taken for Raman analysis. $[Fe(6\text{-}Me_3\text{-}TPA)(BF)]^+$ ^{18}O-labeled only at the carboxyl group was obtained by adding $H_2{}^{16}O$ to a CH_3CN solution of the fully ^{18}O-labeled BF complex. The selectively ^{18}O-labeled complexes with $Fe(II)(Tp^{Ph2})$ were similarly obtained except that a 9:1 mixture of CH_2Cl_2/CH_3CN was used.

Physical Methods. UV/vis spectra were recorded on an HP 8453A diode array spectrometer. Low-temperature visible spectra were obtained using an immersion dewar equipped with quartz windows. Resonance Raman spectra were collected on an Acton AM-506 spectrometer (2400-groove grating) using a Kaiser Optical holographic supernotch filter with a Princeton Instruments liquid N_2-cooled (LN-1100PB) CCD detector with 4 cm^{-1} spectral resolution. The laser excitation lines were obtained with a Spectra Physics 2030-15 argon ion laser and a 375B CW dye (Rhodamine 6G), or a Spectra Physics BeamLok 2060-KR-V krypton ion laser. The Raman frequencies were referenced to indene, and the entire spectral range of 400−1700 cm^{-1} was obtained by collecting spectra at 2−3 different frequency windows and splicing the spectra together. For the model complexes, the spectra were obtained with 200 mW power at 77 K using a backscattering geometry on samples frozen on a gold-plated copper coldfinger in thermal contact with a dewar containing liquid N_2. Typical accumulation times were 16−32 min per frequency window. The Raman spectra of the TauD samples were obtained at room temperature by 90° scattering in an airtight spinning cell. Typical accumulation times were 3−6 h per frequency window. Curve fits (Gaussian functions) and baseline corrections (polynomial fits) were carried out using Grams/32 Spectral Notebase Version 4.04 (Galactic).

Results

Resonance Raman Studies of TauD. TauD is an *E. coli* enzyme that degrades taurine to sulfite and aminoacetaldehyde in the presence of Fe(II), α-KG, and O_2.[12,13] Fe(II)TauD itself is colorless, but the addition of Fe(II) and α-KG to TauD under anaerobic conditions results in the appearance of a purple color with a broad absorption band centered near 530 nm (Figure 1A and Table 1).[22] This chromophore has been attributed to three metal-to-ligand charge-transfer (MLCT) transitions from the Fe(II) center to α-KG, suggesting that α-KG chelates the iron center.[20,23] The resonance Raman spectrum of the Fe(II)TauD-(α-KG) complex was obtained by excitation (568.2 nm) into this absorption band (Figure S5, Supporting Information). The quality of the spectra obtained from these samples is diminished by the presence of a high fluorescence background that is also present in the apo-enzyme. In addition, the low intensity of the MLCT bands (ϵ = 140 M^{-1} cm^{-1}) leads to only a weak enhancement of the vibrations associated with the chromophore.

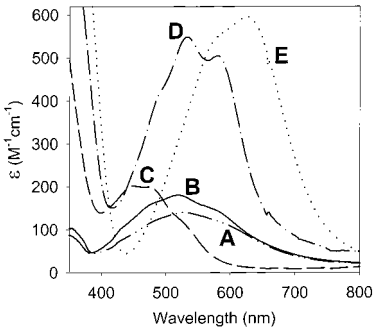

Figure 1. Electronic spectra of Fe(II)−α-keto acid complexes showing the metal-to-ligand charge-transfer transitions. Unless noted, all spectra were recorded at room temperature. (A) Fe(II)TauD(α-KG) (—••—); (B) Fe(II)TauD(α-KG) + taurine (—); (C) $[Fe(II)(Tp^{Ph2})(PRV)]$ in CH_2Cl_2 (– – –); (D) $[Fe(II)(Tp^{Ph2})(BF)]$ in CH_2Cl_2 (—•—); (E) $[Fe(II)(Tp^{Ph2})(BF)]$ in CH_2Cl_2 at −40 °C with 500 equiv of pyridine (•••).

Table 1. Electronic Spectral Features of Fe−α-Keto Acid Complexes in the Visible Region

complex	visible absorption [nm (ϵ (M^{-1} cm^{-1}))]	ref
Fe(II)TauD(α-KG)	490 (sh), 530 (140), 585 (sh)	22
Fe(II)TauD(α-KG)(taurine)	480 (sh), 520 (180), 580 (sh)	22
$[Fe(II)(Tp^{Ph2})(BF)]$	480 (sh, 390), 531 (540), 584 (sh, 500)	this work
$[Fe(II)(6\text{-}Me_3\text{-}TPA)(BF)]^+$	495 (sh, 550), 544 (690), 590 (sh, 600)	23
$[Fe(II)(Tp^{Ph2})(PRV)]$	441 (210), 479 (210), 525 (sh, 120)	this work
$[Fe(II)(6\text{-}Me_3\text{-}TPA)(PRV)]^+$	broad weak shoulder between 450 and 600 nm	this work

The full Raman spectra (400−1750 cm^{-1}) of apo-TauD and Fe(II)TauD(α-KG) (Figure S5, Supporting Information) show numerous common features between 700 and 1700 cm^{-1} which arise from the protein[32,33] and water.[34] Comparison of the Raman spectra of Fe(II)TauD(α-KG) and apo-TauD between 400 and 600 cm^{-1} (Figure 2A,B), however, shows a significantly more intense feature at 460 cm^{-1} in Fe(II)TauD(α-KG) than in the absence of iron(II) and α-KG. This feature at 460 cm^{-1} occurs in the region expected for a metal−ligand stretching vibration.[35] In the region between 1200 and 1800 cm^{-1}, no prominent new features are observed due to the numerous protein and water vibrations (Figure S5, Supporting Information). Subtraction of the spectrum of apo-TauD from the spectrum of Fe(II)TauD-(α-KG) reveals a new feature at 1686 cm^{-1}, which is in the region expected for a C═O vibration.[35] The same feature at 1686 cm^{-1} was observed in the difference spectrum of Fe(II)-TauD(α-KG) versus the same sample after the purple chromophore had decayed upon exposure to air (Figure 2B). In general, the difference spectra obtained by using the air-decayed sample as a control had a better signal-to-noise ratio due to the comparability of the fluorescence backgrounds. This high fluorescence background also prevented us from obtaining a reliable excitation profile for the 460 and 1686 cm^{-1} features.

(32) Lord, R. C.; Yu, N.-T. *J. Mol. Biol.* **1970**, *50*, 509−524.
(33) Loehr, T. M.; Sanders-Loehr, J. *Methods Enzymol.* **1993**, *226*, 431−470.
(34) Spiro, T. G.; Czernuszewicz, R. S. *Methods Enzymol.* **1995**, *246*, 416−460.
(35) Nakamoto, K. *Infrared and Raman Spectra of Inorganic and Coordination Compounds. Part B: Applications in Coordination, Organometallic, and Bioinorganic Chemistry*; John Wiley & Sons: New York, 1997; pp 54−56, 74−77.

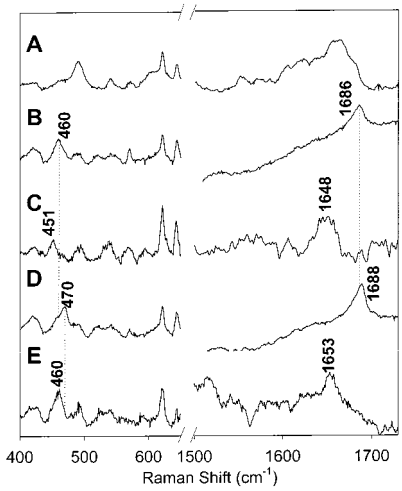

Figure 2. Resonance Raman spectra of TauD samples. (A) apo-TauD; (B) Fe(II)TauD(α-KG); (C) Fe(II)TauD(α-KG) in $H_2{}^{18}O$; (D) Fe(II)-TauD(α-KG) + taurine; (E) Fe(II)TauD(α-KG) + taurine in $H_2{}^{18}O$. The Raman spectra in the lower frequency region were baseline corrected. In the upper frequency region, the spectrum of apo-TauD was baseline corrected, while the other spectra were obtained by subtracting from the raw spectrum the spectrum of the same sample after air oxidation to decompose the purple chromophore. In the case of spectrum C, the subtracted data were also baseline corrected. All the spectra were obtained with 568.2 nm laser excitation using 90° scattering geometry from an anaerobic spinning cell at room temperature.

^{18}O-labeled samples were prepared to assign these two Raman features, presumably due to the binding of the α-KG to the iron(II) center. The resonance Raman spectrum of Fe(II)TauD(α-KG) in $H_2{}^{18}O$ buffer shows that the feature at 460 cm^{-1} shifts to 451 cm^{-1} and that the 1686 cm^{-1} feature is replaced by a broad peak at 1648 cm^{-1} (Figure 2C). The fact that both vibrations shift in the $H_2{}^{18}O$ sample suggests that ^{18}O is incorporated into the α-KG and that the features at 460 and 1686 cm^{-1} are associated with the Fe(II)−α-KG chromophore. A more definitive assignment of these two features can be made on the basis of the results of the model studies discussed in the next section.

The effect of adding the primary substrate, taurine, was investigated as well. Previous spectroscopic studies of TauD reported that the addition of taurine to Fe(II)TauD(α-KG) caused the λ_{max} to blue shift (Figure 1 and Table 1), suggesting that α-KG remains chelated, but with some change in the iron coordination environment.[22] The Raman spectrum of Fe(II)-TauD(α-KG) + taurine shows features at 470 and 1688 cm^{-1} (Figure 2D) which downshift by 10 and 35 cm^{-1}, respectively, upon ^{18}O labeling (Figure 2E). Relative to the corresponding features of the binary complex, the C═O stretch is only slightly perturbed by the addition of taurine, but the metal−ligand vibration upshifts by 10 cm^{-1}. An interpretation for this upshift will be presented in the Discussion section.

Resonance Raman Spectra of Model Complexes. Previously, we reported the crystal structures of two iron(II) complexes with chelating benzoylformate (BF), the five-coordinate [Fe(II)(Tp^{Ph2})(BF)][27] and the six-coordinate [Fe(II)-(6-Me_3-TPA)(BF)]$^+$.[23] Both of these complexes are purple-blue in color with three absorption bands in the visible region centered near 550 nm (Figure 1D and Table 1). The corresponding complexes with pyruvate instead of BF show three absorption bands centered near 470 nm for the Fe(II)(Tp^{Ph2}) complex (Figure 1C and Table 1) and a broad band around 500 nm for the Fe(II)(6-Me_3-TPA) complex. The observed blue shift

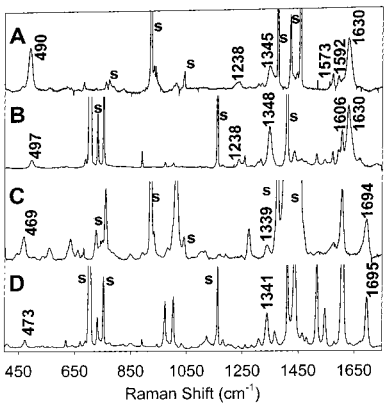

Figure 3. Resonance Raman spectra of Fe−α-keto acid model complexes. (A) [Fe(II)(6-Me_3-TPA)(BF)]$^+$ in CH_3CN; (B) [Fe(II)-(Tp^{Ph2})(BF)] in CH_2Cl_2; (C) [Fe(II)(6-Me_3-TPA)(PRV)]$^+$ in CH_3CN; (D) [Fe(II)(Tp^{Ph2})(PRV)] in CH_2Cl_2. The labeled features are the only ones that are resonance enhanced. All the spectra were obtained at 77 K using a backscattering geometry with 568.2 nm laser excitation for the BF complexes and 514.5 nm for the pyruvate complexes. Solvent bands are labeled with an "s".

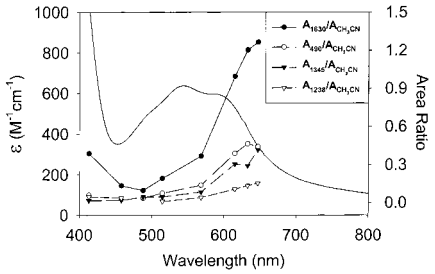

Figure 4. Electronic spectrum of [Fe(II)(6-Me_3-TPA)(BF)]$^+$ and resonance Raman excitation profiles for the 490, 1238, 1345, and 1630 cm^{-1} features. The internal references used for the excitation profiles are the 922 cm^{-1} CH_3CN band for the 490 cm^{-1} feature and the 1376 cm^{-1} CH_3CN band for the 1238, 1345, and 1630 cm^{-1} features. The areas were obtained by curve fitting.

in the electronic spectra upon replacement of the phenyl group in BF with the more electron-donating methyl group in pyruvate is consistent with the assignment of these bands as arising from metal-to-ligand charge-transfer transitions.

The resonance Raman spectra of the four complexes were obtained (Figure 3). The Raman spectrum of [Fe(II)(6-Me_3-TPA)(BF)]$^+$ in CH_3CN obtained with 568.2 nm excitation at 77 K (Figure 3A) shows three prominent nonsolvent features at 490, 1345, and 1630 cm^{-1}, with weaker features at 1238, 1573, and 1592 cm^{-1}. The excitation profile of [Fe(II)(6-Me_3-TPA)(BF)]$^+$ (Figure 4) confirms that these features are associated with the charge-transfer band near 550 nm. The wavelength at which resonance enhancement is maximum appears red-shifted relative to the absorption maximum; such a red shift has been noted for other complexes as well.[36,37] Corresponding features at 497, 1348, and 1630 cm^{-1} are observed in the Raman spectrum of [Fe(II)(Tp^{Ph2})(BF)], with additional peaks at 1238 and 1606 cm^{-1} (Figure 3B). The pyruvate complexes exhibit corresponding features near 470, 1340, and 1690 cm^{-1}, which are weakly enhanced due to the lower extinction coefficients of these complexes (Figure 3C,D). The spectra of the pyruvate complexes show more vibrational features, which may arise

(36) Sanders-Loehr, J.; Wheeler, W. D.; Shiemke, A. K.; Averill, B. A.; Loehr, T. M. *J. Am. Chem. Soc.* **1989**, *111*, 8084−8093.
(37) Dong, Y.; Ménage, S.; Brennan, B. A.; Elgren, T. E.; Jang, H. G.; Pearce, L. L.; Que, L., Jr. *J. Am. Chem. Soc.* **1993**, *115*, 1851−1859.

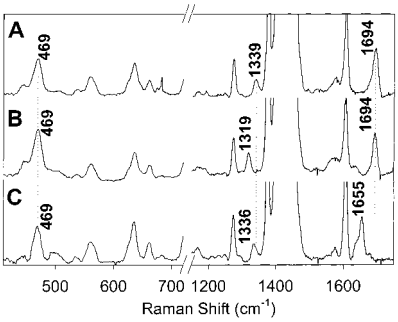

Figure 5. Resonance Raman spectra of ^{13}C-labeled [Fe(II)(6-Me$_3$-TPA)(PRV)]$^+$. (A) [Fe(II)(6-Me$_3$-TPA)(PRV)]$^+$ in CH_3CN; (B) with 1-^{13}C-labeled pyruvate; (C) with 2-^{13}C-labeled pyruvate. All the spectra were obtained at 77 K using a backscattering geometry with 457.9 nm laser excitation.

from the vibrations of the 6-Me$_3$-TPA or Tp^{Ph2} ligand due to the use of higher energy excitation (514.5 or 457.9 nm).

The features near 470−490, 1240, 1350, and 1630−1695 cm^{-1} are associated with vibrations of the iron(II)−α-keto acid chromophore on the basis of isotope labeling experiments. The Raman spectra of [Fe(II)(6-Me$_3$-TPA)(PRV)]$^+$ with ^{13}C-labeled pyruvate show that the high-frequency features downshift while the 469 cm^{-1} mode remains unaffected. The feature at 1339 cm^{-1} in the unlabeled sample (Figure 5A) shifts significantly to 1319 cm^{-1} (Figure 5B) with 1-^{13}C labeling, indicating that this feature is associated with the carboxyl group. Similarly, the feature at 1694 cm^{-1} in the unlabeled sample can be assigned to the C═O vibration of the α-keto carbonyl group since it downshifts by 39 cm^{-1} in the spectrum of [Fe(II)(6-Me$_3$-TPA)-(2-$^{13}C_2$−PRV)]$^+$ (Figure 5C). The 1339 cm^{-1} feature also downshifts slightly (3 cm^{-1}) with this isotopomer, suggesting that a C1−C2 bond deformation is a component of this vibration. This finding is consistent with IR studies of [Fe(III)(oxalate)$_3$]$^{3-}$, where a 1390 cm^{-1} feature was assigned to a combination of ν_s(C−O) and ν(C−C) modes.[38] These results strongly suggest that the 1350 and 1630−1690 cm^{-1} features can be associated, respectively, with the carboxyl and α-keto carbonyl groups of the coordinated α-keto acid.

The Raman spectra of ^{18}O-labeled [Fe(II)(Tp^{Ph2})(BF)] complexes (Figure 6A,B) show that the features at 497, 1238, 1348, and 1630 cm^{-1} are affected by ^{18}O incorporation. For the "fully" labeled complex, the features at 1238 and 1348 cm^{-1} downshift by 9 and 11 cm^{-1}, respectively, while the 497 and 1630 cm^{-1} features show more complicated changes (Figure 6B). With ^{18}O labeling, the feature at 1630 cm^{-1} mostly disappears, as features at 1566, 1589, and 1606 cm^{-1} all increase in intensity. The enhancement of three new features with ^{18}O labeling may be due to the coupling of the C═^{18}O stretch with vibrations from the phenyl ring of comparable energy. The small shoulders that persist at 1348 and 1630 cm^{-1} in the ^{18}O-labeled complex indicate that the carboxyl and α-keto carbonyl groups are not completely labeled, consistent with the 95% enrichment of ^{18}O in the water and the NMR observations (Figures S1−S4, Supporting Information). Compared to the unlabeled samples, the Raman spectrum of [Fe(II)(Tp^{Ph2})(^{18}O-BF)] also shows a complete loss of the 497 cm^{-1} peak and its replacement by two new features at 465 and 478 cm^{-1}. Since neither the carboxyl nor the α-keto carbonyl group is fully ^{18}O-labeled, the lack of a residual peak at 497 cm^{-1} suggests that this feature cannot be associated with ν(Fe−O$_{carboxyl}$) or ν(Fe−O$_{carbonyl}$) alone, but rather is associated with a mode that involves both keto and carboxylate oxygens. As a consequence, the features at 465 and 478 cm^{-1} are proposed to correspond to the fully and partially labeled complexes, respectively.

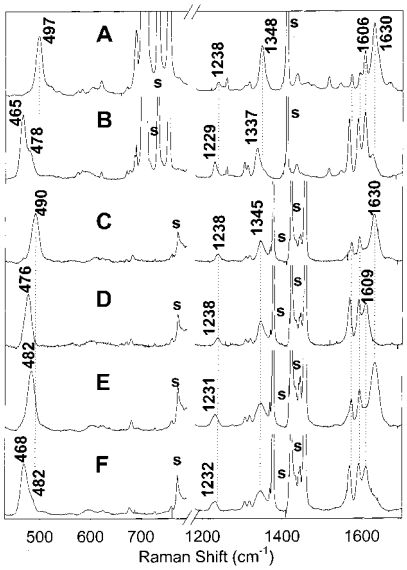

Figure 6. Resonance Raman spectra of ^{18}O-labeled complexes of [Fe(II)(Tp^{Ph2})(BF)] and [Fe(II)(6-Me$_3$-TPA)(BF)]$^+$. (A) [Fe(II)(Tp^{Ph2})(BF) in CH_2Cl_2; (B) "fully labeled" [Fe(II)(Tp^{Ph2})(^{18}O-BF) in CH_2Cl_2; (C) [Fe(II)(6-Me$_3$-TPA)(BF)]$^+$ in CH_3CN + 100 equiv of $H_2{}^{16}O$; (D) [Fe(II)(6-Me$_3$-TPA)(BF)]$^+$ in CH_3CN + 100 equiv of $H_2{}^{18}O$; (E) "fully labeled" [Fe(II)(6-Me$_3$-TPA)(^{18}O-BF)]$^+$ in CH_3CN + 100 equiv of $H_2{}^{16}O$; (F) "fully labeled" [Fe(II)(6-Me$_3$-TPA)(^{18}O-BF)]$^+$ in CH_3CN. All the spectra were obtained at 77 K using a backscattering geometry with 615.0 nm laser excitation. Solvent bands are labeled with an "s".

The assignment of the 460−500 cm^{-1} feature as a coupled vibration involving ν(Fe−O$_{carboxyl}$) and ν(Fe−O$_{carbonyl}$) modes was verified with samples ^{18}O-labeled at only the α-keto carbonyl or carboxyl group. Since $H_2{}^{18}O$ exchange should occur faster at the α-keto carbonyl group than at the carboxyl group, initial attempts to ^{18}O-label selectively the α-keto carbonyl group were carried out by dissolving pyruvic or benzoylformic acid in $H_2{}^{18}O$ for short periods of time and/or lower temperatures. Under all conditions tried, NMR studies showed that ^{18}O labeling occurred at both groups; therefore, the selectively ^{18}O-labeled complexes could not be directly synthesized by this approach. Subsequently, selective labeling of the keto group was achieved by adding $H_2{}^{18}O$ to solutions of the iron(II)−α-keto acid complexes. The Raman spectrum (Figure 6D) of an acetonitrile solution of [Fe(II)(6-Me$_3$-TPA)(BF)]$^+$ with added $H_2{}^{18}O$ shows that the ν(C═O)$_{carbonyl}$ at 1630 cm^{-1} (for a similarly prepared $H_2{}^{16}O$ sample, Figure 6C) completely disappears and is replaced by three peaks at 1566, 1589, and 1609 cm^{-1}, while the feature associated with the carboxyl group at 1345 cm^{-1} is unaffected. The feature at 490 cm^{-1} also shifts to 476 cm^{-1}. This result indicates that, when BF is bound to the iron(II) center, only the α-keto carbonyl group exchanges with $H_2{}^{18}O$. Even after 1 week of equilibration between [Fe(II)(6-Me$_3$-TPA)(BF)]$^+$ with $H_2{}^{18}O$ at room temperature, no exchange at the carboxyl group was observed. This selective labeling of the α-keto carbonyl group was also observed with [Fe(II)(6-Me$_3$-TPA)(PRV)]$^+$ in CH_3CN and [Fe(II)(Tp^{Ph2})(PRV)] using a 9:1 ratio of CH_2Cl_2 and CH_3CN as the solvent (Table 2).

The [Fe(II)(6-Me$_3$TPA)(BF)]$^+$ complex ^{18}O-labeled only at the carboxyl group was obtained by treating the fully ^{18}O-labeled complex with $H_2{}^{16}O$ (Figure 6E). As expected, the feature at 1630 cm^{-1} did not shift, but the feature at 1238 cm^{-1} shifted to 1231 cm^{-1} when the carboxyl group was labeled (Figure

(38) Fujita, J.; Martell, A. E.; Nakamoto, K. *J. Chem. Phys.* **1962**, *36*, 324−331.

Table 2. Observed Resonance Raman Features of Fe(II)−α-Keto Acid Complexes.

complexes	observed resonance Raman features (cm^{-1})						
	$\nu_{(Fe-O)}$	$\nu_{(COO)sym}$	$\nu_{(COO)asym}$				$\nu_{(C=O)}$
Fe(II)TauD(α-KG)	460						1686
in $H_2{}^{18}O$	451						1648
+ taurine	470						1688
+ taurine in $H_2{}^{18}O$	460						1653
$[Fe(II)(6\text{-}Me_3\text{-}TPA)(BF)]^{+}$ [a]	490	1238	1345	1573	1592		1630
^{18}O-keto carbonyl	476	1238	1345	1566	1589		1609
^{18}O-carboxylate	482	1231	1345	1573	1592		1630
^{18}O-BF	468, 482 (sh)	1232	1345	1566	1589		1609
$Fe(II)(Tp^{Ph2})(BF)$ [b]	497	1238	1348	1573	1592	1606	1630
^{18}O-BF	465, 478 (sh)	1229	1337	1566	1589		1609
+ 1-methylimidazole	477	1238	1351	1571	1591	1606	1626
+ pyridine	483	1238	1352	1573	1592	1606	1623
+ CH_3CN	488	1238	1352	1573	1592	1606	1629
+ 2,6-lutidine	497	1238	1348	1573	1592	1606	1630
$[Fe(II)(6\text{-}Me_3\text{-}TPA)(PRV)]^{+}$ [a]	469		1339				1694
1-^{13}C	469		1319				1694
2-^{13}C	469		1336				1655
^{18}O-keto carbonyl	463		1339				1667
$Fe(II)(Tp^{Ph2})(PRV)$ [b]	473		1341				1695
1-^{13}C	473		1321				1695
2-^{13}C	473		1338				1655
+ CH_3CN	463		1345				1693
+ CH_3CN + $H_2{}^{18}O$	454		1345				1663

[a] In CH_3CN. [b] In CH_2Cl_2.

6E,F). The feature at 1345 cm^{-1} did not shift in any of the ^{18}O-labeled samples of $[Fe(II)(6\text{-}Me_3\text{-}TPA)(BF)]^{+}$, but it did broaden significantly when the carboxyl group was labeled. The 490 cm^{-1} feature is also downshifted, but only by 8 cm^{-1}, compared to a downshift of 14 cm^{-1} observed when only the α-keto group is labeled. In the fully labeled complex, a downshift of 22 cm^{-1} is observed, which is the sum of the shifts observed for the selectively labeled complexes. These results clearly demonstrate that the feature at 490 cm^{-1} can be assigned to a vibration involving both the keto carbonyl and a carboxylate oxygen, one perhaps analogous to the chelate mode observed in iron−catecholate complexes[39,40] at ca. 520 cm^{-1} and $[Fe(III)(oxalate)_3]^{3-}$ [38] at 498 cm^{-1}.

Effect of Coordination Number. A comparison of the Raman spectra of the six-coordinate $[Fe(II)(6\text{-}Me_3\text{-}TPA)(\alpha\text{-keto acid})](ClO_4)$ and the five-coordinate $[Fe(II)(Tp^{Ph2})(\alpha\text{-keto acid})]$ complexes shows small shifts in the resonance-enhanced Raman vibrations (Table 2 and Figure 3). The largest difference (6 or 7 cm^{-1}) is observed for the ν(Fe−O) feature of the BF complexes, suggesting a slightly stronger binding of the α-keto acid to iron in the five-coordinate iron center in the Tp^{Ph2} complex than to the six-coordinate center in the 6-Me_3-TPA complex. This is also consistent with the shorter bond lengths usually associated with five-coordinate complexes over six-coordinate complexes. However, the small shifts in the vibrations of the 6-Me_3-TPA and Tp^{Ph2} complexes may simply reflect inherent differences between the two ligands.

To determine more systematically if the iron coordination number affected the properties of bidentate α-keto acid complexes, the effect of adding a potential sixth ligand to $[Fe(II)(Tp^{Ph2})(BF)]$ was explored. The addition of 1-methylimidazole or pyridine to a CH_2Cl_2 solution of $[Fe(II)(Tp^{Ph2})(BF)]$ at room temperature resulted in no change in the visible spectrum. However, at −40 °C, addition of 5 equiv of 1-methylimidazole or 500 equiv of pyridine induced a red shift of the bands near 530 nm (Figure 1D) of $[Fe(II)(Tp^{Ph2})(BF)]$ to one broad band centered near 610 nm (Figure 1E). Interestingly, only 1 equiv of either base was required to induce the color change in frozen solutions at 77 K. A similar color change is observed upon freezing a $CH_2Cl_2-CH_3CN$ (9:1) solution of $[Fe(II)(Tp^{Ph2})(BF)]$. Thus, lower temperatures favor the six-coordinate adduct. The observed red shifts upon formation of the adducts are consistent with a metal center with diminished Lewis acidity that gives rise to a lower energy MLCT transition.

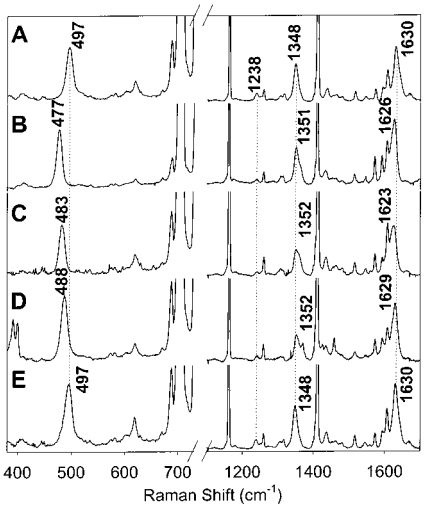

Figure 7. Resonance Raman spectra of $[Fe(II)(Tp^{Ph2})(BF)]$ with addition of a sixth ligand. (A) $[Fe(II)(Tp^{Ph2})(BF)]$ in CH_2Cl_2; (B) $[Fe(II)(Tp^{Ph2})(BF)]$ + 1 equiv of 1-methylimidazole in CH_2Cl_2; (C) $[Fe(II)(Tp^{Ph2})(BF)]$ + 1 equiv of pyridine in CH_2Cl_2; (D) $[Fe(II)(Tp^{Ph2})(BF)]$ in a 9:1 mixture of CH_2Cl_2 and CH_3CN; (E) $[Fe(II)(Tp^{Ph2})(BF)]$ + 1 equiv of 2,6-lutidine in CH_2Cl_2. All the spectra were obtained at 77 K using a backscattering geometry with 615.0 nm laser excitation.

$$[Fe(Tp^{Ph2})(BF)] + L \rightleftharpoons [Fe(Tp^{Ph2})(BF)L]$$

The addition of 1-methylimidazole, pyridine, or CH_3CN to $[Fe(II)(TP^{Ph2})(BF)]$ also causes significant changes in the Raman spectra (Table 2 and Figure 7). Of these three ligands studied, the most basic, 1-methylimidazole (Figure 7B), induces the largest downshift of the feature at 497 cm^{-1}. The apparent trend that the stronger ligand results in a greater weakening of the

(39) Salama, S.; Stong, J. D.; Neilands, J. B.; Spiro, T. G. *Biochemistry* **1978**, *218*, 3781−3785.
(40) Michaud-Soret, I.; Andersson, K. K.; Que, L., Jr. *Biochemistry* **1995**, *34*, 5504−5510.

Fe(II)−α-KG acid interaction is consistent with the formation of six-coordinate adducts. Aside from the 497 cm^{-1} feature, smaller changes in ν(C═O) (1630 cm^{-1}) and the feature at 1348 cm^{-1} are also noted in the six-coordinate adducts (Table 2 and Figure 7). On the other hand, the addition of 2,6-lutidine resulted in no changes in the appearance of the Raman spectrum (Figure 7E). Though it is a stronger base than pyridine, the steric bulk of 2,6-lutidine presumably prevents it from binding to the iron center to give a six-coordinate complex. From these results, the resonance Raman spectra of Fe(II)−α-keto acid complexes are shown to be sensitive to the coordination number of the iron center.

Discussion

The studies presented above clearly demonstrate that resonance Raman spectroscopy is an effective probe of the Fe(II)−α-keto acid chromophore. Based on the model studies, the resonance Raman signature for these complexes consists of a strong feature above 1600 cm^{-1} associated with the C═O vibration from the α-keto carbonyl group and two weaker features near 460−500 and 1350 cm^{-1} that are associated with a metal−ligand mode and the carboxyl group, respectively. The strong resonance enhancement of the 1600 cm^{-1} feature is consistent with the notion that the chromophore involves the low-lying π^* orbital of the α-keto carbonyl group, resulting in a large C═O bond deformation in the excited state. This observation supports a recent molecular orbital description proposed by Solomon et al. on the origin of the metal-to-ligand charge-transfer transitions in iron(II)−α-keto acid complexes.[20] The 460−500 cm^{-1} feature is assigned to a deformation of the five-membered chelate ring, as indicated by the sensitivity of this feature to ^{18}O labeling of both the carboxyl and α-keto carbonyl groups. The appearance of this coupled vibration also provides direct evidence for the binding of both the carboxyl and α-keto carbonyl groups to the iron center. The well-enhanced Raman features of the BF complexes are not as pronounced in the pyruvate complexes (Figure 3 and Table 2), which may be attributed to the lower extinction coefficient of the pyruvate complexes. The resonance Raman spectrum of the Fe(II)TauD(α-KG) complex exhibits only two discernible features at 460 and 1686 cm^{-1}, due to its low extinction coefficient, the high fluorescence background, and overlapping protein vibrations.

The model studies provide the basis for interpreting the resonance Raman spectra of TauD. The Raman spectrum of the Fe(II)TauD(α-KG) complex shows two features at 460 and 1686 cm^{-1} (Figure 2B), both of which are significantly shifted in $H_2{}^{18}O$ (Figure 2C). These two features are assigned to the chelate ring mode and the $C{=}O_{carbonyl}$ stretch, respectively.[41] The downshift of only 9 cm^{-1} for the 460 cm^{-1} feature in the $H_2{}^{18}O$ sample is much lower than the downshifts of 22 and 32 cm^{-1} observed in the fully ^{18}O-labeled BF complexes (Table 2), suggesting that the α-KG is labeled only at either the carboxyl or the α-keto carbonyl group. Since the 1686 cm^{-1} feature is downshifted by 36 cm^{-1} in the $H_2{}^{18}O$ sample (Table 2), it is likely that only the α-keto carbonyl oxygen exchanged with $H_2{}^{18}O$, similar to the observation in the model studies. We note that the 9 cm^{-1} downshift observed for Fe(II)TauD(α-KG) is comparable to the 6−9 cm^{-1} downshifts observed for the pyruvate complexes when the keto oxygen is ^{18}O-labeled (Table 2). Therefore, these results indicate that the α-keto carbonyl is bound to the iron and confirm the chelation of α-KG to iron(II), as initially suggested by the observed electronic transitions.

Scheme 2. Proposed Mechanism for Selective $^{18}O^-$ Labeling at the α-Keto Carbonyl Group in [Fe(II)(L)(α-Keto Acid)]$^{n+}$ Complexes with $H_2{}^{18}O$

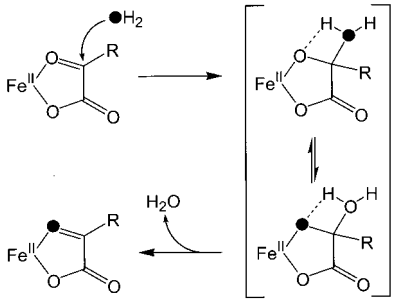

When the substrate, taurine, is added to the Fe(II)TauD(α-KG) complex, the chelate ring and $C{=}O_{carbonyl}$ vibrations are still observed (Figure 2D), indicating that α-KG remains chelated to the iron, but the chelate ring vibration shifts to higher energy. This upshift may suggest a change in the iron coordination number from six to five, from a comparison with the Raman data on model complexes (Table 2). Such a decrease in the iron coordination was also observed in MCD studies of the Fe(II)-CAS(α-KG) complex upon addition of substrate,[42] and in the crystal structure of Fe(II)CAS(α-KG) in the presence of proclavaminic acid.[16] This change in coordination number upon the addition of taurine would open up a coordination site for O_2.

We and others have described the putative O_2 adduct to be an iron(III) superoxide complex and have proposed that the oxidative decarboxylation of α-KG is initiated by nucleophilic attack on the keto carbon by the bound superoxide.[4,18,19] The susceptibility of the bound keto carbon to nucleophilic attack is demonstrated by the facile exchange of $H_2{}^{18}O$ into the keto group in both the model complexes and TauD. This exchange (Scheme 2) most likely occurs by the attack of $H_2{}^{18}O$ on the keto carbon to generate a *gem*-diol intermediate. Such an attack would be promoted by coordination of the keto oxygen to the Lewis acidic iron(II) center, which would enhance the electrophilicity of the keto carbon.

In summary, resonance Raman spectroscopy can serve as a useful probe for the iron(II)−α-keto acid chromophore in models and α-KG-dependent dioxygenases. The Raman features of the chelated iron(II)−α-KG complex can be readily observed and are sensitive to the metal coordination number of the metal center. Furthermore, the $H_2{}^{18}O$ exchange reactions show that the keto carbon of the α-keto acid is particularly prone to nucleophilic attack. These results provide useful insights into the initial steps of the mechanism of α-KG-dependent enzymes.

Acknowledgment. This work was supported by the National Institutes of Health (Grant GM-33162 to L.Q., Postdoctoral Fellowship GM-20196 to M.J.R., Postdoctoral Fellowship GM-

(41) The alternative assignment of the 460 cm^{-1} peak to ν(Fe−OH) or ν(Fe−OH_2) can be excluded for a number of reasons: (a) Based on a Hooke's law calculation, ν(Fe−O) would be expected to downshift 20 cm^{-1} upon ^{18}O labeling; only a 9 cm^{-1} downshift is observed. (b) The large downshift observed for ν(C═O) is inconsistent with a ν(Fe−OH) or a ν(Fe−OH_2) assignment. (c) ν(Fe−O) still persists upon binding of taurine, the primary substrate binding, despite the expected loss of the solvent ligand as observed in the crystal structure of Fe(II)CAS(α-KG) in the presence of proclavaminic acid[16] and deduced from MCD studies of CAS.[42] (d) It is more likely that an Fe−OH_2 moiety is present in Fe(II)TauD(α-KG), given the presence of two anionic ligands and the usual preference for charge neutrality in a metalloprotein active site; ν(Fe−OH_2), however, is generally observed below 400 cm^{-1}.[35]

(42) Zhou, J.; Gunsior, M.; Bachmann, B. O.; Townsend, C. A.; Solomon, E. I. *J. Am. Chem. Soc.* **1998**, *120*, 13539−13540.

18639 to E.L.H., and Predoctoral Traineeship GM-08700 to M.P.M.) and the National Science Foundation (Grant 9603520 to R.P.H.)

Supporting Information Available: ^{1}H and ^{13}C NMR spectra of the ^{18}O-labeled ligands; full resonance Raman spectra of the apo-TauD and Fe(II)TauD(α-KG) complexes reported herein (PDF). This material is available free of charge via the Internet at http://pubs.acs.org.

JA0041775

RECEIVED MAR 2 6 2001

Ho, R. Y. N.; Mehn, M. P.; Hegg, E. L.; Liu, A.; Ryle, M. J.; Hausinger, R. P.; Que, L., Jr. "Resonance Raman Studies of the Iron(II)-α-Keto Acid Chromophore in Model and Enzyme Complexes," *J. Am. Chem. Soc.*

Supporting Information

NMR Spectra of ^{18}O-Labeled α-Keto Acids. The presence of pyruvic acid and its hydrate are indicated both in the ^{1}H and ^{13}C NMR spectra (Fig. S1). Despite the lack of referencing to an internal standard, the ^{13}C spectrum clearly illustrates the 0.04 ppm upfield shift expected due to ^{18}O substitution at both the ketonic and the carboxylic acid positions (Fig. S2). Furthermore, it appears that the majority of the oxygens are labeled in the α-keto position and a mixture of zero, one and two labeled oxygens have been incorporated at the carboxylic acid positions for both pyruvic acid and the *gem*-diol. The *gem*-diol peak at approximately 90 ppm also shows a splitting due to the incorporation of ^{18}O-label. The same procedure has been carried out with benzoylformic acid though longer time periods (2 wks) were required for incorporation to occur. Some decomposition has occurred over the course of labeling but the majority of the sample remains benzoylformic acid (Fig. S3). This impurity appears to be benzoic acid. and the ^{13}C NMR spectrum is consistent with that assignment. Analysis of the ^{13}C NMR spectrum of benzoylformic acid in $H_2{}^{18}O$ shows similar incorporation of ^{18}O into both the α-keto and carboxylic acid functionalities though the splitting is not as well resolved (Fig. S4). This proves that the α-keto acid has indeed been labeled, and furthermore gives an indication of the positions that have been labeled and the extent of labeling.

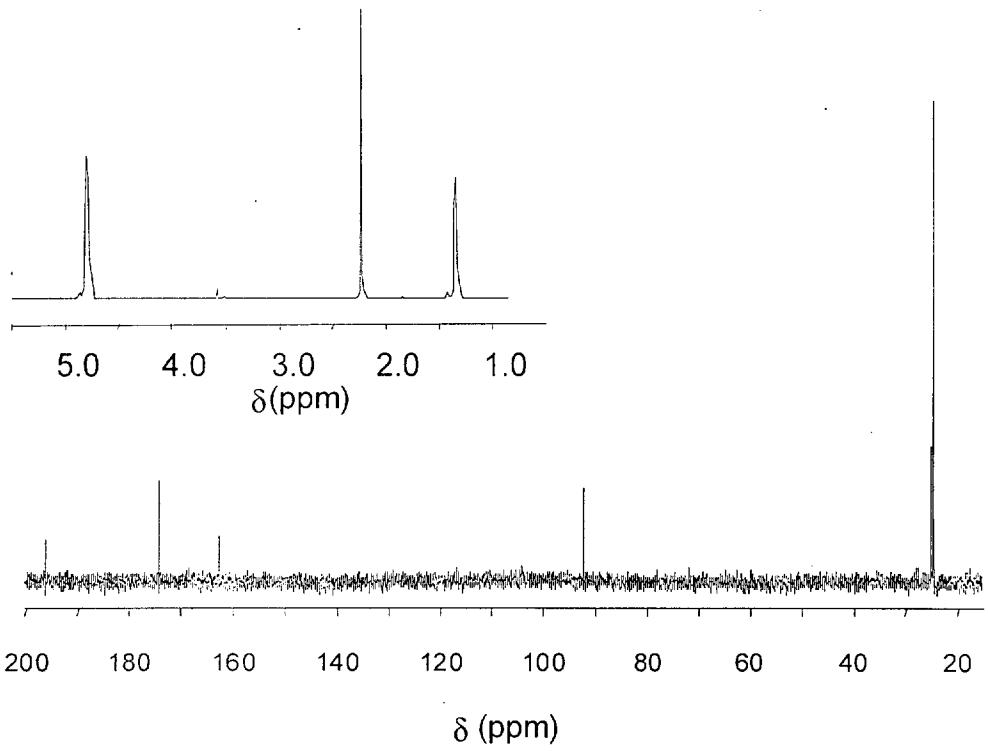

Figure S1. ^{1}H and ^{13}C NMR spectra of 1.5 M pyruvic acid in $H_2{}^{18}O$ after seven days. The proton spectrum is referenced to the water peak at 4.81 ppm and the ^{13}C spectrum is not referenced. The presence of pyruvic acid and its gem diol is evident from the presence of the *gem*-diol peak at 90 ppm, the splitting of the methyl resonance, and the extra carboxylic acid peak at 175 ppm.

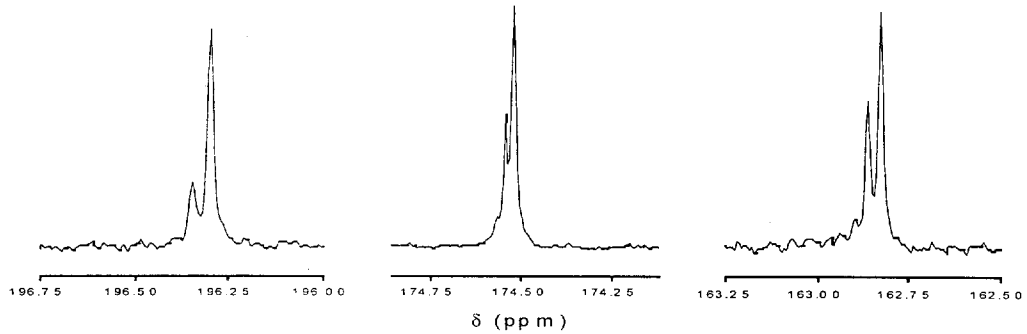

Figure S2. ^{13}C NMR spectrum of the pyruvic acid in labeled water after 7 days. The ketonic region (196 ppm), the carboxylic acid peaks from the *gem*-diol (174 ppm) and the carboxylic acid of pyruvic acid (163 ppm) all indicate multiple incorporations of label after seven days of exchange.

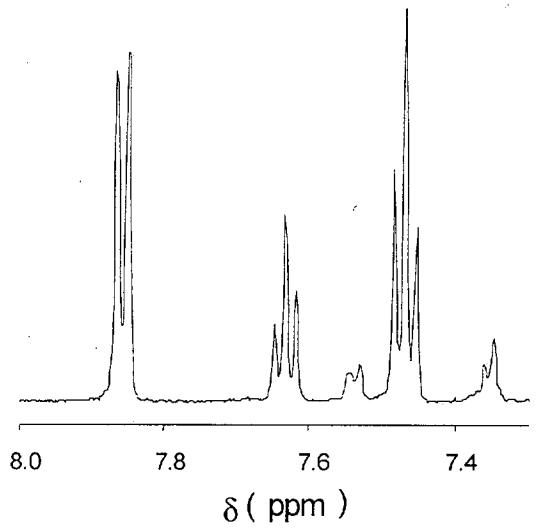

Figure S3. ^{1}H NMR spectrum of benzoylformic acid after 2 weeks of equilibration with $H_2{}^{18}O$ referenced to the water peak. Solvent suppression was used to obtain the above spectrum.

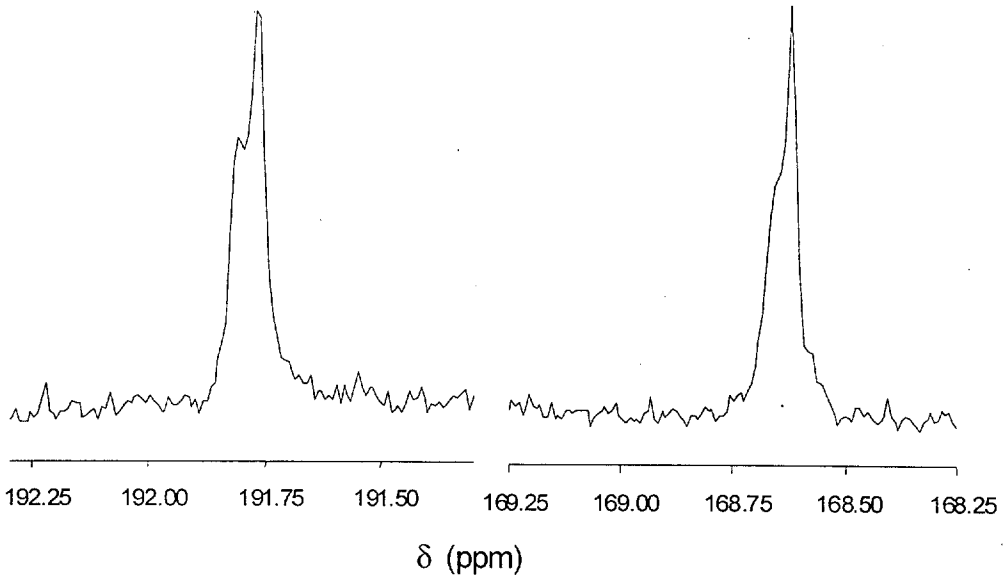

Figure S4. ^{13}C NMR spectrum of the ketonic (192 ppm) and carboxylic acid (168 ppm) peaks observed for the ^{18}O-labeled benzoylformic acid solution. The intensities have been maximized in each region.

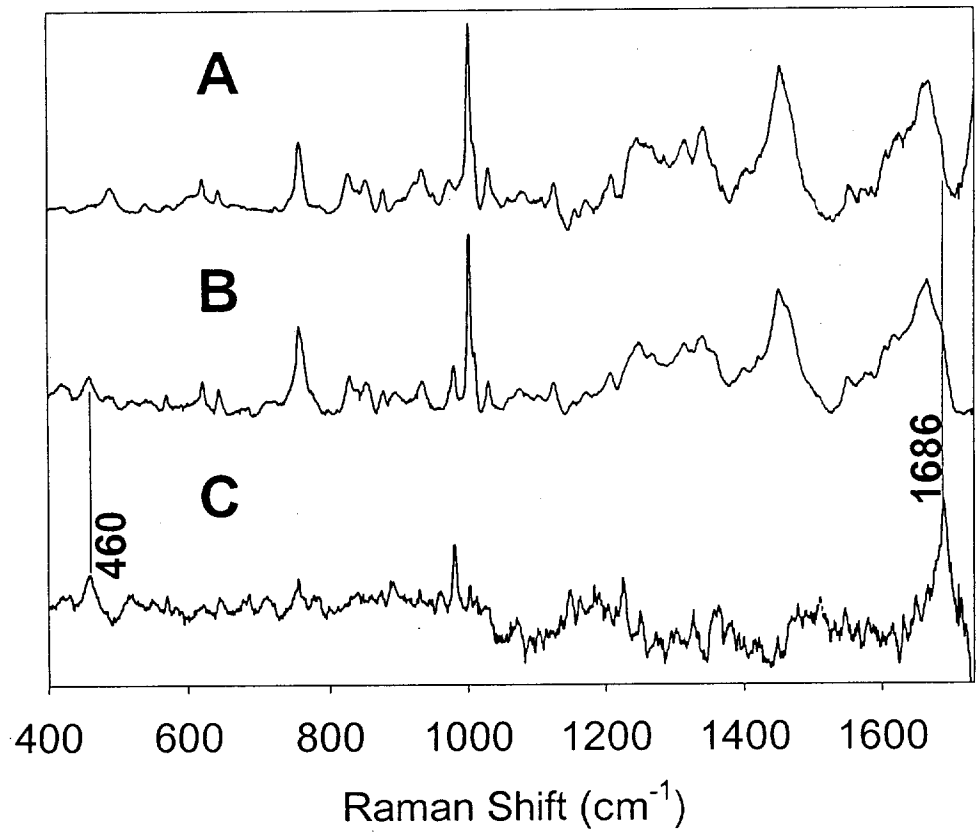

Figure S5. Full resonance Raman spectra of apo-TauD and Fe(II)TauD(α-KG). A) Apo-TauD, B) Fe(II)TauD(α-KG), C) Spectrum B- Spectrum A. The Raman spectra were baseline corrected using a function fit in Grams32. The Raman frequencies were referenced to indene and the frequency range of 400-1700 cm^{-1} was obtained by collecting spectra at 2 different frequency windows and splicing the spectra together. For C the percent subtraction was based on removing the tryptophan ring mode at 760 cm^{-1} (for lower frequency region) and the C-H deformation modes around 1450 cm^{-1} from the protein. All the spectra were obtained using 90° scattering geometry from an anaerobic spinning cell at room temperature with 568.2 nm laser excitation.